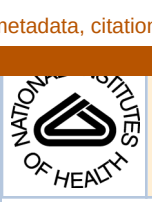

Published in final edited form as:

J Magn Reson Imaging. 2009 May ; 29(5): 1035–1042. doi:10.1002/jmri.21734.

Improved Cerebellar Tissue Classification on Magnetic Resonance Images of Brain

Sushmita Datta, PhD[1,*], **Guozhi Tao, PhD**[1], **Renjie He, PhD**[1], **Jerry S. Wolinsky, MD**[2], and **Ponnada A. Narayana, PhD**[1]

[1] Department of Diagnostic and Interventional Imaging, University of Texas Medical School at Houston, 6431 Fannin Street, Houston, TX 77030

[2] Department of Neurology, University of Texas Medical School at Houston, 6431 Fannin Street, Houston, TX 77030

Abstract

Purpose—To develop and implement a method for improved cerebellar tissue classification on the magnetic resonance images of brain by automatically isolating the cerebellum prior to segmentation.

Materials and Methods—Dual fast spin echo (FSE) and fluid attenuation inversion recovery (FLAIR) images were acquired on eighteen normal volunteers on a 3 T Philips scanner. The cerebellum was isolated from rest of the brain by using a symmetric inverse consistent nonlinear registration of individual brain with the parcellated template. The cerebellum was then separated by masking the anatomical image with individual FLAIR images. Tissues in both the cerebellum and rest of the brain were separately classified using hidden Markov random field (HMRF), a parametric method, and then combined to obtain tissue classification of the whole brain. The proposed method for tissue classification on real magnetic resonance (MR) brain images was evaluated subjectively by two experts. The segmentation results on Brainweb images with varying noise and intensity nonuniformity levels were quantitatively compared with the ground truth by computing the Dice similarity indices.

Results—The proposed method has significantly improved the cerebellar tissue classification on all normal volunteers included in this study without compromising the classification in remaining part of the brain. The average similarity indices for gray matter (GM) and white matter (WM) in the cerebellum are 89.81 (± 2.34) and 93.04 (± 2.41), demonstrating excellent performance of the proposed methodology.

Conclusion—The proposed method significantly improved tissue classification in the cerebellum. The GM was overestimated when segmentation was performed on the whole brain as a single object.

Keywords

Magnetic resonance imaging; Segmentation; Brain; Cerebellum

Introduction

The cerebellum plays a strategic role in the central nervous system. It weighs approximately 10% of the brain, but contains more neurons and circuitry than rest of the brain (1). The

[*]Corresponding Author: Department of Diagnostic and Interventional Imaging, University of Texas Medical School at Houston, 6431 Fannin Street, Houston, TX 77030, Phone: (713)500-7677, Fax: (713)500-7684, Email: Sushmita.Datta@uth.tmc.edu.

cerebellum has been studied extensively in recent years for its involvement in various pathologies and aging. MacKenzie-Graham et al (2) have found direct correlation between cerebellar cortical atrophy and disease duration in experimental autoimmune encephalomyelitis, an experimental model of multiple sclerosis (MS). Change in the cerebellar volume has also been associated with various neurological disorders such as autism, Alzheimer, Parkinson, Huntington, schizophrenia, and MS (3–7). In elderly brains normal aging results in more white matter (WM) loss compared to gray matter (GM) in cerebellum and cerebrum (7). Similarly, extensive demyelination of cerebellar GM is shown to occur in MS. Therefore, accurate classification of cerebellar tissues is important in understanding the relationship between tissue atrophy and clinical status.

Magnetic resonance imaging (MRI) allows acquisition of images with different contrasts by altering the pulse sequences and/or acquisition parameters. The multi-modal nature of MRI has been widely exploited for tissue classification and tissue volumetry (9–16). The majority of tissue classification schemes depends on image intensity and assumes that a given tissue has the same intensity, independent of its location. However, this is not always true. Suckling et al (14) have reported inferior GM-WM distinction in the cerebellum compared to other parts in the brain, when the segmentation is performed with the whole brain considered as a single object. They attributed the tissue misclassification in cerebellum to image contrast nonuniformity arising from the edge of the transmit/receive coil. Recent studies also point out intensity differences between the cerebellum and rest of the brain (17). The spatial dependent intensity pattern leads to misclassification of tissues when the whole brain is segmented. The intensity nonuniformity correction alone is not adequate to address this problem. For minimizing the tissue misclassification, Suckling et al (14) have divided the whole brain into overlapping rectangular windows followed by separate classification in each window. The sizes of these windows are determined by an interactive procedure that allows operator to select certain number of slices to be included in each window. Also, adjacent window would have common slices so that the classification information can be used for spatial dependency within each tissue. The choice of the rectangular window size is not trivial as the shape and size of cerebellum exhibit considerable inter-subject variability. Lewis and Fox (18) have reported differences in relative intensities in the cerebellar tissues between two scans on the same subject. Such an intensity change affects longitudinal assessment of tissue volume changes and other quantitative measures. These authors have applied differential nonuniformity correction to minimize the intensity difference in the cerebellum in serial scans. While this method may be useful for following changes in atrophy at two different time points in serial studies, it may not be applicable for tissue segmentation.

Most of the segmentation procedures are based on T1-weighted images which exhibit excellent GM-WM contrast and delineation of different structures. But, lesions such as those seen in multiple sclerosis (MS) and other pathologies are not clearly visualized on T1 weighted images. However, these lesions are clearly seen on dual FSE and FLAIR images. Therefore, these sequences are commonly used for clinical management of these patients and segmentation of lesions for assessing disease progression (13). Thus, classification of GM and WM along with lesions is important in the analysis of disease progression and atrophy. For these reasons, in the present study we have developed and implemented a method for improved cerebellar tissue classification on dual FSE and FLAIR images.

In order to overcome intensity variation within dual FSE images, the cerebellum was isolated from the brain. The automatic isolation of cerebellum was performed by registering the images to a template using a symmetric inverse consistent nonlinear registration algorithm described elsewhere (19). This was followed by separate segmentation of these regions into GM and WM tissues. In this study, segmentation was performed on 18 normal

brains with the proposed methodology and the results were subjectively assessed by two experts. The method was applied to Brainweb images (http://www.bic.mni.mcgill.ca/brainweb/selection_normal.html; 20) to ensure that our approach did not introduce any tissue misclassification in rest of the brain.

Materials and Methods

Image acquisition

These studies are HIPAA (Health Insurance Portability and Accountability Act) compliant and approved by our institution's Committee for the Protection of Human Subjects. Written informed consent was obtained from each subject prior to imaging.

Eighteen healthy normal volunteers (10 females and 8 males; median age of 29.5 yrs; range: 21–57 yrs) were included in this study. All volunteers underwent MRI on a 3T Philips Intera scanner (Philips Medical System, Best, Netherland) using a six channel receive only head coil with a sensitivity encoding (SENSE) factor of 2. Dual FSE and FLAIR images were acquired with the following parameters: TE1/TE2/TR = 8.2 ms/90 ms/6800 ms, and TE/TI/TR = 80 ms/2600 ms/10002 ms respectively, where TI and TR represent the inversion and repetition times, respectively. TE1, TE2 are the two echo times for the dual FSE images and TE represents the echo time for the FLAIR images. The other parameters were: field-of-view = 240 mm × 240 mm, slice thickness = 3 mm with no gap, and image matrix = 256 × 256. A total of 44 slices were acquired covering the whole brain from foramen magnum to vertex.

Segmentation of Brain

The initial post-processing included rigid body registration of FLAIR with FSE images using the module available in SPM2 (Statistical Parametric Mapping; 21) followed by removal of the extrameningeal tissues with a semi-automated procedure (13,22). Anisotropic diffusion filtration was applied for reducing noise without blurring the edges (23) and intensity nonuniformity was corrected using the module in SPM2 (24). The rigid body registration and intensity nonuniformity correction modules were rewritten in IDL (Interactive Data Language; RSI, Boulder, CO) to integrate with the rest of our software.

The brains were initially classified into parenchyma and cerebrospinal fluid (CSF) based on the T2-weighted (long echo FSE) and FLAIR images using the Parzen window classifier (25), described elsewhere in detail (13). HMRF, a parametric procedure (16), was used on the short echo (proton density- or proton density (PD)-weighted) and T2-weighted FSE images to divide the parenchyma into GM and WM tissue classes.

The cerebellum was automatically separated from rest of the brain using the anatomical image obtained from International Consortium of Brain Mapping (ICBM), known as ICBM single subject MRI anatomical template. This template was produced by averaging 27, T1-weighted MRI acquisitions from a single subject (Montreal Neurological Institute database) and comprises of 56 labels with cerebellum as one of the largest structure (26). This ICBM template and associated anatomical structures were co-registered with the FLAIR images acquired on our subjects using the symmetric inverse consistent registration described elsewhere (19). Briefly, the symmetric inverse consistent registration is based on a symmetric cost function that includes mutual information (MI) as the similarity measure, regularization of transformation, and inverse consistency error (ICE) terms. This method avoids difficulties in balancing the divergent terms in the cost function, similarity measure, regularization of transformation, and inverse consistency error terms were alternatively minimized. As suggested by demons algorithm (27), in this inverse consistency method, an alternate minimization strategy has been implemented to minimize the cost function. Instead

of the squared sum of intensity differences, mutual information is used to drive the registration process to deal with the intensity variations in different image volumes. The composition scheme is adapted for updating the displacement fields to achieve diffeomorphism. The inverse consistency is achieved by forcing the ICE term towards zero (19).

Following registration, the cerebellum of the co-aligned anatomical structure labeled image was masked with the FLAIR image to separate the cerebellum in our dataset. Since the FLAIR and FSE images were co-registered prior to the removal of extrameningeal tissues, the cerebellum mask from FLAIR image was used to isolate the cerebellum on the FSE images.

The parenchymal regions of cerebellum and rest of the brain on the FSE images were segmented separately into GM and WM using the expectation-maximization with HMRF algorithm as described elsewhere in detail (13). The GM-WM tissue classes of the cerebellum and remaining brain were merged with CSF to obtain the final segmentation of the whole brain. The major steps involved in the proposed methodology are summarized in Fig. 1.

Evaluation

The segmentation results of the proposed method were evaluated by two experts, a Neurologist and a Medical Physicist, both with more than 25 years experience in neuroimaging. In the absence of ground truth about the distribution and volumes of these tissues in the brain, the performance of our algorithm was subjectively evaluated on real MR images based on visual inspection. The surrounding CSF in the cerebellar region was excluded through isolation, and therefore, only GM and WM were included in this comparison. The GM and WM tissue volumes were calculated with and without isolating cerebellum to confirm the subjective evaluation. The dual FSE and FLAIR images were segmented using the FAST tool available in the FSL (FMRIB). The segmentation results obtained with proposed methodology were also compared subjectively with the results obtained with FAST tool.

In order to validate the cerebellum isolation approach for segmentation, the proposed method was applied to segment simulated normal MR images obtained from Brainweb (28). Brainweb images were simulated with the same intensity distribution for individual tissues in the whole brain (20). Therefore, the segmentation results are expected to be similar with and without cerebellum isolation. The two-dimensional normal PD- and T2-weighted images with matrix size 181 × 217 comprising of 60 slices with 3 mm slice thickness were used in this study. Noise levels of 1%, 3% and 5%, and intensity nonuniformity of 20% and 40% were added to these images. The segmentation results on these images were quantitatively evaluated based on the Dice similarity index (DSI) (29) defined as:

$$\mathrm{DSI}=\left(\frac{2\times(\mathrm{Seg}\cap\mathrm{Ref})}{\mathrm{Seg}+\mathrm{Ref}}\right)\times 100$$

where, ‘Seg’ represents segmented image obtained with our procedure and ‘Ref’ is the reference image representing the crisp anatomical image from the Brainweb database. To further test the accuracy of segmentation with the proposed method, the individual tissue volumes were compared with those obtained with FAST tool available in the FSL (16) on the Brainweb images.

Results

Segmentation

As an example, Fig. 2 shows histograms of the cerebellum and remaining brain, excluding CSF, derived from the PD- and T2-weighted images. The difference in the histogram peak positions of cerebellum and rest of the brain can easily be seen in this figure.

Figure 3 shows the template (a) and anatomical structure labeled (b) images along with the PD-, T2-weighted (c, d) and FLAIR (e) images of a normal brain. As indicated above, the template image volume was registered to the FLAIR image volume by applying an inverse consistent registration algorithm (19). The cerebellum on FSE and FLAIR images was then extracted by masking the cerebellum structure from the registered labeled image. The isolated cerebellum structures on the FSE and FLAIR images are shown in Figs. 3f–3h.

Figures 4a and 4b show the PD- and T2-weighted and segmented images of two normal volunteers (subjects 9 and 11) obtained with and without isolating the cerebellum. For comparison, the segmented results of FSL are included in column six of Figs. 4a and 4b. Isolation of cerebellum has substantially improved the classification of cerebellar WM. In contrast, WM was underestimated when the tissue classification was performed on the whole brain. In addition, the proposed method provided better delineation of substantia niagra, a GM structure in the midbrain, as can be observed visually from the fourth column of the Fig. 4b. Similar results were observed on all the 18 normal brains included in this study. Figure 5 represents the GM-WM tissue volumes that were calculated on 18 normal brains with and without isolating the cerebellum. It can be observed from this figure that the GM volume was overestimated in cerebellum without its isolation.

Evaluation

The average GM and WM volumes following segmentation with and without the cerebellum isolation on normal brains are summarized in Table 1. The p-values were calculated separately for the cerebellar and rest of the brain regions using Student's two-tailed paired t-test. The paired t-test was used as the segmentation with and without cerebellum isolation was performed on the same set of subjects. The average GM (WM) volume decreased (increased) by 13 cc in the cerebellum following its isolation. Similarly, segmentation with the cerebellum isolation resulted in an average decrease (increase) in the GM (WM) volume by 5 cc in the rest of the brain. The GM and WM volumes with and without the cerebellum isolation were significantly different (p-value < 0.0001) in normal subjects (Table 1), but the total sum remained the same as expected.

The simulated Brainweb PD- and T2-weighted and segmented images, with and without the cerebellum isolation, are shown in Fig. 6. The ground truth and the segmentation results obtained with FSL are also included in this figure. Table 2 summarizes the Dice similarity indices for GM and WM volumes obtained on the Brainweb images with varying noise and intensity nonuniformity levels, with and without the cerebellum isolation from the brain. These measures indicate that the tissue classifications on Brainweb images are not affected by the cerebellum isolation. To compare the accuracy of our method, the similarity indices of the results obtained with FSL are also included in this table. Unlike real MR images, the Brainweb images assume the same tissue intensities in the cerebellum and rest of the brain. These results also demonstrate that the proposed methodology does not introduce any artifacts in GM and WM classifications.

Discussion

We have proposed and implemented a method for improved segmentation of GM and WM in the whole brain by isolating the cerebellum. The proposed methodology was evaluated by comparing the segmentation results with and without isolation. Our method is completely automatic except for the removal of extrameningeal tissues (a semi-automated procedure) which requires some manual intervention procedure. The other fully automated steps include 1) image pre-processing, 2) nonlinear inverse consistent registration of template anatomical labeled image with FLAIR image, 3) isolation of cerebellum from brain, 4) segmentation, and 5) integration of all tissue classes from cerebellum structure and remaining brain.

Our results on 18 normal subjects showed remarkable improvement in GM-WM classification following the cerebellum isolation from rest of the brain. The WM tissue in cerebellum was observed to be underestimated when the whole brain was segmented into different tissues as a single object. The isolation prior to segmentation has resulted in WM volume increase of 13 cc (~30%) in the cerebellum (table 1), and has increased only 2% of WM volume in rest of the brain. In addition, Fig. 5 clearly confirms the subjective assessment of consistent underestimation of WM in the cerebellum of all the normal brains without cerebellum isolation. A significant improvement in the cerebellar tissue classification on real MR images was observed without any influence on the classification in rest of the brain (Fig. 4) as judged by the two experts. Thus, cerebellum isolation provides better tissue classification without compromising the classification in rest of the brain.

The Brainweb MR images are generated by simulation (20) and do not take into account the intensity differences between the cerebellum and remaining brain. Therefore, as expected, GM-WM volumes in the cerebellum are not affected by cerebellar isolation (Fig. 6; Table 2). Also, these results demonstrate that our segmentation procedure, like FSL, is relatively insensitive to small noise and intensity nonuniformity. As expected, these results show that the performance of segmentation degrades with increased noise and intensity nonuniformity levels.

Accurate classification of tissues is important since in diseases such as MS, atrophy of individual tissues, rather than the whole brain volume, is thought to correlate better with the clinical status (2,30–34). The segmentation of lesions and WM and GM in neurological diseases such as MS plays an important role towards identification of biomarker of the disease. Often, the tissue classification is found to be significantly inferior in the cerebellum in the presence of pathology when the segmentation is performed on the whole brain assuming it as a single object. Our main aim is to implement the proposed method on images acquired in multi-center clinical trials. We have implemented the proposed methodology on dual FSE and FLAIR images as these images are routinely acquired in many neurological diseases as part of clinical management of patients. We intend to extend the application of the proposed methodology to include lesion class along with other tissue classes for segmentation of diseased brains.

The proposed method automatically takes into account shape and size of the cerebellum by separating it from the brain without any human intervention, thus facilitating independent segmentations of the two brain regions. It has been shown that the inverse consistent nonlinear registration algorithm used in co-registering the normal brain with the template is diffeomorphic (19). The registration procedure applied to IBSR dataset (Internet Brain Segmentation Repository) (19,35) showed high similarity index of 0.95 for cerebellum structure when isolated from the whole brain as compared to the ITK demons (27) and B-spline based deformation model (36). This suggests that there is a maximum of 5% error in

isolating the cerebellum structure from the brain caused by nonlinear registration used in this study which would have relatively low impact on the cerebellar segmentation.

As observed from Fig. 3, the automated isolation of cerebellum was obtained by excluding the brain stem. The Dice similarity index of cerebellum was found to be 95% with the use of nonlinear registration algorithm. Although the cerebellar volume was somewhat underestimated, the automated procedure was adapted to isolate the cerebellum to minimize the operator bias involved in manual procedure. Also, the manual procedure is not feasible when large number of image volumes need to be analyzed as in multi-center clinical trials.

In conclusion, we have proposed a scheme for segmenting the whole brain by isolating the cerebellum prior to GM and WM tissue classification. The overall improvement in the tissue classification was judged by experts subjectively. The efficacy of this method was demonstrated quantitatively on Brainweb MR images with varying noise and intensity nonuniformity.

Acknowledgments

Grant Support: National Institutes of Health Grant EB002095 to PAN

The authors thank Mr. Vipul Kumar Patel for acquiring MR images on 3T Philips Intera scanner.

References

1. Houk, JC.; Mugnani, E. Cerebellum. In: Squire, LR.; Roberts, JL.; Spitzer, NC.; Zigmond, MJ.; McConnell, SK.; Bloom, FE., editors. Fundamental Neuroscience. 2. New York: Academic Press; 2003. p. 841-872.
2. MacKenzie-Graham A, Tinsley MR, Shah KP, et al. Cerebellar cortical atrophy in experimental autoimmune encephalomylitis. NeuroImage. 2006; 32:1016–1023. [PubMed: 16806982]
3. Fennema-Notestine C, Archibald SL, Jacobson MW, et al. In vivo evidence of cerebellar atrophy and cerebral white matter loss in Huntington disease. Neurology. 2004; 63:989–995. [PubMed: 15452288]
4. Hayashi N, Sanada S, Suzuki M, et al. Semiautomated volumetry of the cerebrum, cerebellum-brain stem, and temporal lobe on brain magnetic resonance images. Radiat Med. 2008; 26:104–114. [PubMed: 18301988]
5. Shin S-E, Lee J-S, Kang M-H, Kim C-E, Bae J-N, Jung G. Segmented volumes of cerebrum and cerebellum in first episode schizophrenia with auditory hallucinations. Psych Res Neuroimaging. 2005; 138:33–42.
6. Bendfeldt K, Kuster P, Traud S, et al. Association of regional gray matter volume loss and progression of white matter lesions in multiple sclerosis - a longitudinal voxel-based morphometry study. Neuroimage. 2008 (In press).
7. Gilmore CP, Donaldson I, Bo L, Owens T, Lowe JS, Evangelou N. Regional variations in the extent and pattern of grey matter demyelination in multiple sclerosis: a comparison between the cerebral cortex, cerebellar cortex, deep grey matter nuclei and the spinal cord. J Neurol Neurosurg Psychiatry. 2008 (In press).
8. Jernigan TL, Archibald SL, Fennema-Notestine C, et al. Effects of age on tissues and regions of the cerebrum and cerebellum. Neurobiol Aging. 2001; 22:581–594. [PubMed: 11445259]
9. He R, Datta S, Sajja BR, Narayana PA. Generalized fuzzy clustering for segmentation of multi-spectral magnetic resonance images. Comput Med Imag Graph. 2008; 32:353–366.
10. Van Leemput K, Maes F, Vandermeulen D, Suetens P. Automated model-based tissue classification of MR images of the brain. IEEE Trans Med Imaging. 1999; 18:897–908. [PubMed: 10628949]
11. Liew AWC, Yan H. Current methods in the automatic tissue segmentation of 3D magnetic resonance brain images. Current Med Imag Rev. 2006; 2:91–103.

12. Pham DL, Prince JL. Adaptive fuzzy segmentation of magnetic resonance images. IEEE Trans Med Imaging. 1999; 18:737–752. [PubMed: 10571379]
13. Sajja BR, Datta S, He R, et al. Unified approach for multiple sclerosis lesion segmentation on brain MRI. Annals of Biomed Engg. 2006; 34:142–151.
14. Suckling J, Sigmundsson T, Greenwood K, Bullmore ET. A modified fuzzy clustering algorithm for operator independent brain tissue classification of dual echo MR images. Magn Reson Imaging. 1999; 17:1065–1076. [PubMed: 10463658]
15. Wells WM, Grimson WEL, Kikinis R, Jolesz FA. Adaptive segmentation of MRI data. IEEE Trans Med Imaging. 1996; 15:429–442. [PubMed: 18215925]
16. Zhang Y, Brady M, Smith S. Segmentation of brain MR images through a hidden random Markov field model and the expectation-maximization algorithm. IEEE Trans Med Imaging. 2001; 20:45–57. [PubMed: 11293691]
17. Datta, S.; Sajja, BR.; He, R.; Dieber, JM.; Narayana, PA. Segmentation of MR brain images with intensity correction and partial volume averaging. Proceedings of the 16th Annual Meeting of ISMRM; Toronto. 2008. (abstract 3165)
18. Lewis EB, Fox NC. Correction of differential intensity inhomogeneity in longitudinal MR images. NeuroImage. 2004; 23:75–83. [PubMed: 15325354]
19. Tao, G.; He, R.; Datta, S.; Narayana, PA. Mutual information driven inverse consistent nonlinear registration. Proceedings of 30th Annual Meeting of IEEE EMBS; Vancouver. 2008. p. 3957-3960.
20. Kwan RKS, Evans AC, Pike GB. An extensible MRI simulator for post-processing evaluation. Lecture Notes in Comp Sc. 1996; 1131:135–140.
21. Ashburner J, Neelin P, Collins DL, Evans A, Friston K. Incorporating prior knowledge into image registration. NeuroImage. 1997; 6:344–352. [PubMed: 9417976]
22. Datta S, Sajja BR, He R, Wolinsky JS, Gupta RK, Narayana PA. Segmentation and quantification of black holes in multiple sclerosis. NeuroImage. 2006; 29:467–474. [PubMed: 16126416]
23. Perona P, Malik J. Scale-space and edge detection using anisotropic diffusion. IEEE Trans Patt Anal Mach Intell. 1990; 12:629–639.
24. Ashburner, J. Another MRI bias correction approach. NeuroImage; Proceedings of 8th International Conference on Functional Mapping of the Human Brain; Sendai. 2002. abstract 10255
25. Duda, RO.; Hart, PE.; Stork, DG. Pattern Classification. New York: John Wiley and Sons; 2001. p. 654
26. ICBM, International Consortium of Brain Mapping. http://www.loni.ucla.edu/ICBM/Downloads/Downloads_ICBMtemplate.shtml
27. Thirion JP. Image matching as diffusion process: an analogy with Maxwell's demons. Med Image Anal. 1998; 2:243–260. [PubMed: 9873902]
28. Cocosco C, Kollokian V, Kwan R-S, Evans A. Brainweb: online interface to a 3D MRI simulated brain database. NeuroImage. 1997; 5:S425.
29. Anbeek P, Vincken KL, van Osch MJP, Bisschops RHC, van der Grond J. Probabilistic segmentation of white matter lesions in MR imaging. NeuroImage. 2004; 21:1037–1044. [PubMed: 15006671]
30. Fisniku LK, Chard DT, Jackson JS, et al. Gray matter atrophy is related to long-term disability in multiple sclerosis. Ann Neurol. 2008; 64:247–254. [PubMed: 18570297]
31. Sim ME, Lyoo IK, Streeter CC, et al. Cerebellar gray matter volume correlates with duration of cocaine use in cocaine-dependent subjects. Neuropshychopharmacology. 2007; 32:2229–2237.
32. Nakamura K, Fisher E. Segmentation of brain magnetic resonance images for measurement of gray matter atrophy in multiple sclerosis patients. Neuroimage. 2009; 44:769–776. [PubMed: 19007895]
33. Altmann DR, Jasperse B, Barkhof F, et al. Sample sizes for brain atrophy outcomes in trials for secondary progressive multiple sclerosis. Neurology. 2008 (In press).

34. Zacharaki EI, Kanterakis S, Bryan RN, Davatzikos C. Measuring brain lesion progression with a supervised tissue classification system. Med Image Comput Comput Assist Interv Int Conf Med Image Comput Comput Assist Interv. 2008; 11:620–627. [PubMed: 18979798]

35. IBSR, Internet Brain Segmentation Repository (IBSR), the Center for Morphometric Analysis at Massachusetts General Hospital. MR brain images and their manual segmentations, http://www.cma.mgh.harvard.edu/ibsr/.

36. Rueckert D, Sonoda LI, Hayes C, Hill DLG, Leach MO, Hawkes DJ. Non-rigid registration using free-form deformations: Application to breast MR images. IEEE Trans Med Imaging. 1999; 18:712–721. [PubMed: 10534053]

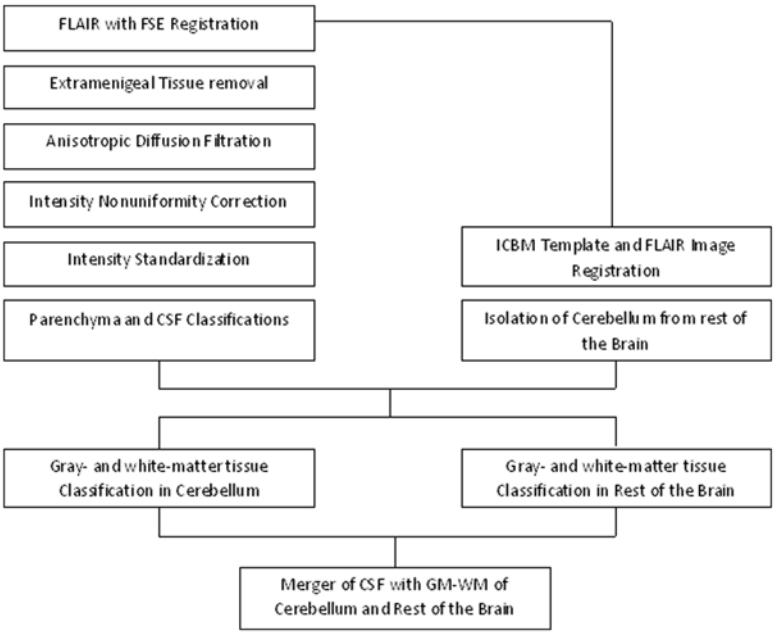

Figure 1.
Flow chart showing major steps of the proposed method.

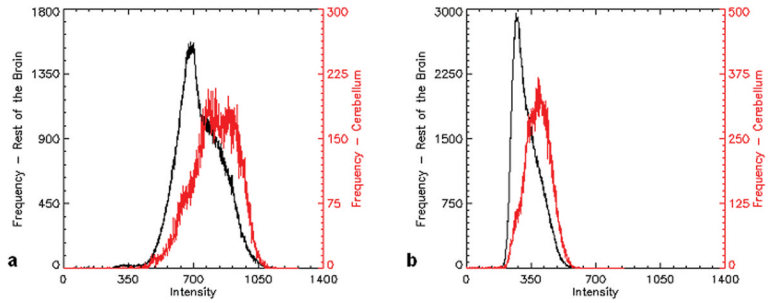

Figure 2.

Histograms of cerebellum (red) and cerebrum (black) excluding CSF: (a) PD- and (b) T2-weighted images on a normal volunteer. Note that the histogram peaks have different locations for the cerebellum and cerebrum.

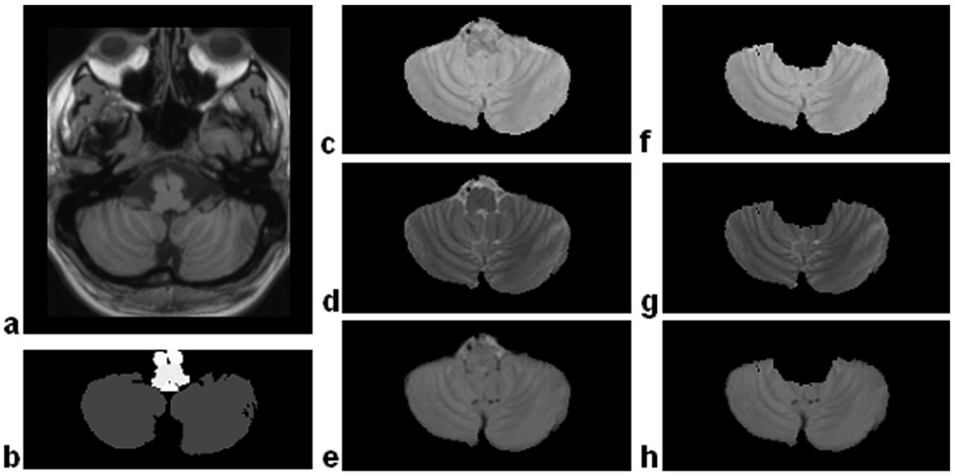

Figure 3.

(a) Template image, (b) anatomical structures of the template image, (c) PD-weighted, (d) T2-weighted image, and (e) FLAIR image of a normal subject; f–h: PD-, T2-weighted and FLAIR images obtained by masking the registered anatomical labeled image following nonlinear registration of the template image to the FLAIR image.

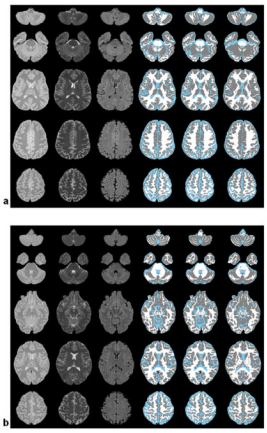

Figure 4.
Segmentation results on two volunteers (subjects 9 and 11) are shown in (a) and (b) respectively. PD-weighted (column 1), T2-weighted (column 2), and FLAIR images (column 3) at different levels. The corresponding segmented images with and without isolating the cerebellum are shown in columns 4 and 5, respectively. Segmentation results of FSL are shown in column 6. The overall improvement in the segmentation of WM and deep GM structures (particularly putamen) with the cerebellum isolation can easily be appreciated. Color scheme: GM – gray, WM – white, CSF – blue.

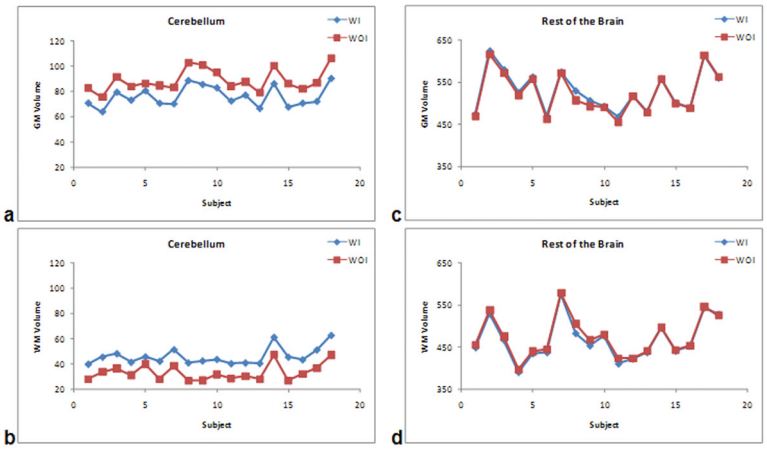

Figure 5.
GM (a) and WM (b) tissue volumes in cerebellum with and without isolation. The corresponding volumes in rest of the brain are shown in (c) and (d). (WI: segmentation with cerebellum isolation (blue); WOI: segmentation without cerebellum isolation (red)).

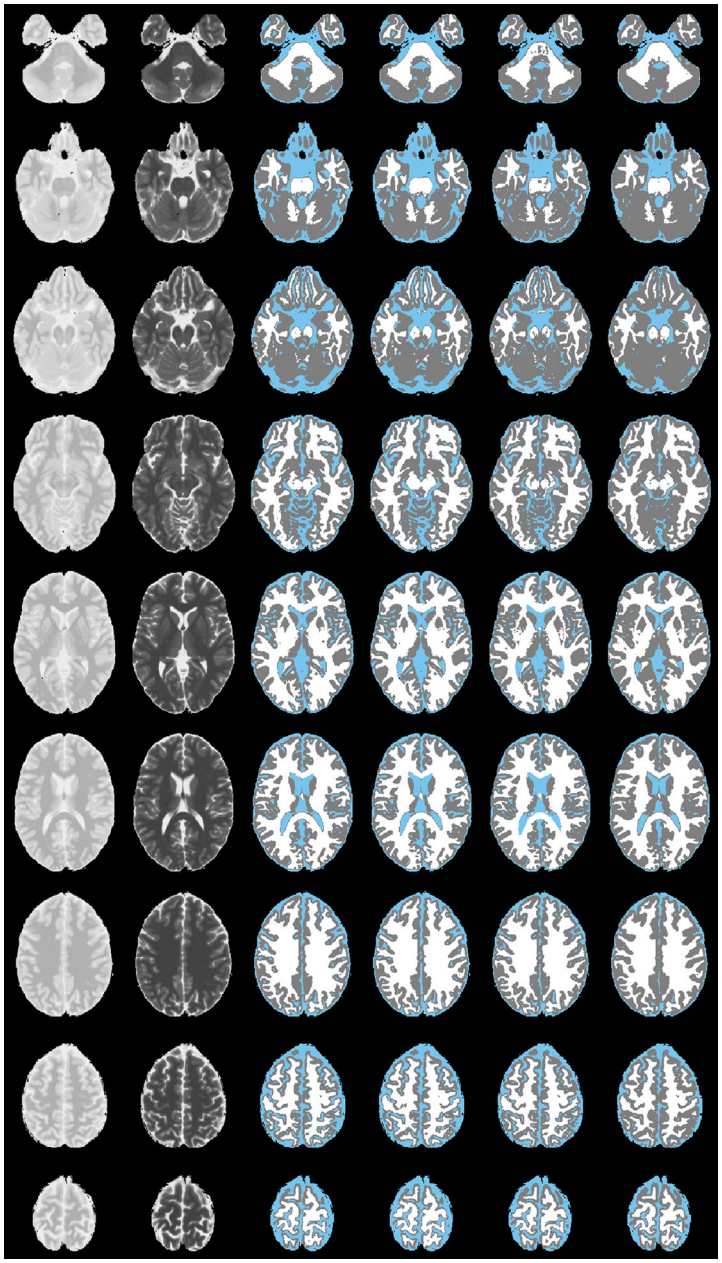

Figure 6.
PD-weighted (first column) and T2-weighted (column 2) images from Brainweb at different levels. The corresponding segmented images with and without cerebellum isolation are shown in columns 3 and 4, respectively. The ground truth is shown in column 5. Segmented images using the FSL on the whole brain are shown in column 6. Since, the Brainweb images do not assume any spatial dependence of intensity for a given tissue, as expected, the segmentation results with and without cerebellum isolation are very similar. Also note that the similarity indices of segmentations obtained with proposed methodology appear to be similar to that obtained with FSL, attesting to the accuracy of our segmentation method. The color scheme is same as in Fig. 4.

Table 1

Volumes of GM and WM in the cerebellum and rest of the brain on 18 normal subjects with and without cerebellum isolation (WI and WOI). The p-values for the volume differences between the two methods are also shown in this table.

	Cerebellum (in cc)			Rest of the Brain (in cc)		
Tissue	**WI**	**WOI**	**p-value**	**WI**	**WOI**	**p-value**
Gray Matter	76.30 ± 8.25	88.96 ± 8.85	$p < 0.0001$	532.70 ± 48.23	527.24 ± 49.62	0.0025
White Matter	46.25 ± 6.85	33.64 ± 6.53	$p < 0.0001$	469.10 ± 50.79	474.80 ± 49.92	0.0014

Table 2

Dice similarity indices for GM-WM tissues obtained with (WI) and without (WOI) the isolation of cerebellum using our procedure and FSL on the Brainweb images.

		GM			WM		
Noise (in %)	**RF (in %)**	**WI**	**WOI**	**FSL**	**WI**	**WOI**	**FSL**
1	20	92.16	91.481	91.978	95.767	95.964	95.51
1	40	92.188	91.407	92.237	95.742	95.92	95.227
3	20	89.352	90.988	91.001	93.041	92.895	92.274
3	40	90.961	91.049	91.107	92.934	92.869	92.234
5	20	87.003	89.101	89.877	90.303	90.917	90.715
5	40	87.216	89.294	89.898	90.444	91.149	90.729